Study on the bulk wave radiation of finite-length SAW devices using FEM/BEM*

WANG Weibiao[1]**, ZHANG Xiaodong[1], SHUI Yongan[1], ZHANG De[1] and HAN Tao[2]

(1. State Key Laboratory of Modern Acoustics, Institute of Acoustics, Nanjing University, Nanjing 210093, China; 2. Shanghai Jiaotong University, Shanghai 200030, China)

Received July 27, 2004; revised October 18, 2004

Abstract Based on the distributions of stress and free charge on the interface of the surface acoustic wave (SAW) device calculated with the combination of boundary element method and finite element method (FEM/BEM), the power of each of the three possible bulk waves radiated by the SAW device is calculated, and their contributions to the overall input conductance are separated respectively. Moreover, the formula of angular distributions of their power radiation into the substrate is derived. Consider the effect of mass loading, the resistance density, defined as a scalar, is extended to generalized resistance densities which can be written as three 4×4 tensors and for which the formulas are derived. The bulk wave radiations for a synchronous one-port resonator on 42° Y-rotated $LiTaO_3$ are simulated. It is found that the radiated energy by slow shear wave contributes a very high proportion to input electrical energy in some frequency range.

Keywords: SAW device, bulk wave radiation, FEM/BEM.

When interdigital transducers excite surface acoustic wave (SAW or LSAW), three possible bulk wave modes (BAWs) are excited and radiate into the bulk of substrate. Generally speaking, the radiation of bulk waves can degrade the performance of SAW devices, so it needs to be suppressed.

On the substrates of $LiNbO_3$ and $LiTaO_3$, which are widely used in modern communication systems, radiation of bulk waves is one of the major causes of attenuations. In SAW devices on such substrates, the losses due to bulk waves have a very significant influence on their performance. Most devices have a structure of synchronous or quasi-synchronous electrode distribution. To suppress the bulk wave radiation under such structure, Koskela et al.[1] reported that the velocity of LSAW can be slowed down below the slow shear wave cut-off velocity under appropriate electrode thickness, so that such loss can be suppressed. Hashimoto et al.[2] found an optimal combination of electrode thickness and cut orientation with minimal bulk leakage. In many devices (for example, in DMS filters), the local asynchronous arrangement is inevitable, which would cause bulk wave radiation and increase the loss. Such cases have attracted the attention of SAW designers and researchers[3,4].

Additionally, when the radiated bulk waves are reflected from the substrate bottom and received by the SAW transducers, they can lead to filter response degradations such as passband ripples and sidelobe. Therefore, study on the radiation of bulk waves is important for the design of high performance SAW devices.

Milsom et al. applied Green's function method to analyze finite-length transducers and calculated the bulk wave power and its angular distribution for the first time[5]. We follow this principle and improve it in two aspects. The first is that we use Chebyshev polynomial expansion to replace the uniform space sampling, as Ventura et al. did[6]. The second is that the mass loading effect is taken into consideration, which is important for accurate simulation. In Ref. [7], although mass loading is considered, because pulse function is used as the basis function, too many coefficients are needed to fit the field distribution. It limits the size of the analyzed device to several tens electrodes, which is not feasible for practical devices.

The most accurate and fastest simulation of finite SAW devices by using finite element method combined with boundary element method (FEM/BEM)

* Supported by National Natural Science Foundation of China (Grant Nos. 10074034 and 10304012), and by the State Key Laboratory on Modern Acoustics of Nanjing University

** To whom correspondence should be addressed. E-mail: weibiao_wang@hotmail.com

was proposed by Ventura et al.[6] They only obtain electrical parameters of the devices. We apply the same algebra, but from the solution we can obtain the field distributions upon the interface, and from the field distributions we can get the bulk wave radiation of the device.

In this paper, from the distributions of stress and charge computed by FEM/BEM, the bulk wave radiation of finite-length SAW devices is studied. On a high-end PC, the FEM/BEM model takes about two minutes to simulate a 200 electrode SAW device for each frequency point and has the capability of analyzing SAW devices with a total number of electrodes up to 500.

1 FEM/BEM theory

The FEM/BEM model is proposed by Ventura et al. to meet the need of rigorous simulation tool in designing low-loss bandpass filters[6]. In this method all the acoustical and electrical interactions, as well as mass loading effects, are taken into account. SAW devices with arbitrary electrode structure on substrates with any cut angle can be modeled accurately using this method, including the effects of bulk waves. All electrical and mechanical information can be obtained by performing such simulation for a finite length SAW device, such as the admittance matrix of the device, the distributions of stresses and free charges on the interface between electrodes and substrate, and the distributions of displacements and potential on the surface of substrate.

The piezoelectric substrate is assumed to occupy the whole lower half-space $x_3 \leqslant 0$. The electrodes are arranged parallel to the x_2-axis, and the 2D-assumption $\partial/\partial x_2 = 0$ is made. The SAW propagates along x_1-axis. Considering the effect of mass loading, the relationship between displacement vector $\boldsymbol{u}(x)$, electric potential $\phi(x)$, stresses vector $\boldsymbol{t}_s(x)$ and free charge density $\sigma(x)$ can be written as

$$\begin{bmatrix} \boldsymbol{u}(x) \\ \phi(x) \end{bmatrix} = \int_{-\infty}^{+\infty} \boldsymbol{G}(x - x') \begin{bmatrix} -\boldsymbol{t}_s(x') \\ \sigma(x') \end{bmatrix} \mathrm{d}x'. \quad (1)$$

Here, $\boldsymbol{G}(x)$ is dyadic Green's function, which can be computed from its counterpart $\boldsymbol{G}(k)$ in k (k is wave number) domain by performing a Fourier transform. Let $|k|\,\boldsymbol{G}(k) = \boldsymbol{H}(k)$, so $\boldsymbol{H}(k)$ is independent of frequency. Details of its computation can be found in Ref. [8]. Considering $k = \omega s$ (s is slowness), we have

$$\boldsymbol{G}(x) = \frac{1}{2\pi} \int_{-\infty}^{+\infty} \frac{\boldsymbol{H}(s)}{|s|} \mathrm{e}^{-\mathrm{j}\omega s x} \mathrm{d}s. \quad (2)$$

The distributions of stress and free charge are expanded using the first kind of Chebyshev polynomial on the jth electrode

$$\begin{bmatrix} \boldsymbol{t}_s(x) \\ \sigma(x) \end{bmatrix} = \sum_{n=1}^{N_{\mathrm{chj}}} \begin{bmatrix} \boldsymbol{b}_t \\ b_\sigma \end{bmatrix}_n T_n\left(\frac{x - c_j}{a_j}\right) \Big\backslash \sqrt{1 - \left(\frac{x - c_j}{a_j}\right)^2}, \quad (3)$$

where N_{chj} is the number of Chebyshev polynomials truncated to interpolate stress and charge. c_j and a_j are the center coordinate and half-width of the jth electrode, respectively. Using Eq. (3) and following BEM process, we obtain the linear equations

$$\begin{bmatrix} \boldsymbol{c}_i^u \\ c_i^\phi \end{bmatrix}_m + \begin{bmatrix} 0 \\ 2\pi\varphi\delta_{0m} \end{bmatrix}_m = \sum_{j=1}^{N_e} \sum_{n=1}^{N_{\mathrm{chj}}} Y_{mn}^{ij} \begin{bmatrix} \boldsymbol{b}_j^{t_s} \\ b_j^\sigma \end{bmatrix}_n, \quad i = 1, \cdots, N_e, \quad m = 1, \cdots, N_{\mathrm{chi}}, \quad (4)$$

where $\begin{bmatrix} \boldsymbol{c}_i^u \\ c_i^\phi \end{bmatrix}_m = \int_0^\pi \begin{bmatrix} \boldsymbol{u}(c_i + a_i\cos\theta) \\ \phi(c_i + a_i\cos\theta) \end{bmatrix} \cos(m\theta)\mathrm{d}\theta$, N_e is the total number of electrodes. φ is a reference potential determined by the condition for charge neutrality of the whole structure. The calculation of Y_{mn}^{ij} follows the procedure described in Ref. [6]. Assuming the potential on the ith electrode is ϕ_i, we have $(c_i^\phi)_{m=0} = 2\pi\phi_i$, $(c_i^\phi)_{m\neq 0} = 0$. The relationship between $(\boldsymbol{c}_i^u)_m$ and $(\boldsymbol{b}_i^{t_s})_n$ can be calculated using FEM[6], substituting the results into Eq. (4), hence $(\boldsymbol{c}_i^u)_m$ is eliminated.

The solution of Eq. (4) contains all the electric and mechanical information of the analyzed device: (i) Admittance of each electrode $y_i = (b_i^\sigma)_0/\phi_i$, from which all electric parameters can be calculated. (ii) Substituting the solution into Eq. (3), the distribution of charge and stress can be obtained. (iii) Utilizing the solution, the distributions of displacement and potential can be calculated from Eq. (1).

2 Bulk wave radiation

Using FEM/BEM, we can obtain the distribution of stress and charge from which we will discuss the radiation of bulk waves. In general, an interdigital transducer excites three bulk wave modes radiating into the bulk of substrate: slow shear bulk acoustic wave (SSBAW), fast shear bulk acoustic wave (FBASW) and longitudinal bulk acoustic wave (LBAW). When $x_3 = -\infty$, they are decoupled with

each other. Therefore, the three wave modes can be dealt with separately[5]. At $x_3=-\infty$, integrating the Poynting vector projected on $-x_3$ axis in x_1 domain from $-\infty$ to $+\infty$, then performing a Fourier transform to s domain, the formula of power radiated into substrate for the nth bulk wave is derived:

$$p_n=-\frac{1}{4\pi}W\mathrm{Re}\int_{-s_n}^{s_n}\mathrm{j}\omega^2\ |B_n\ |^2(D_3^{(n)}\varphi^{(n)^*}+\sum_{i=1}^{3}T_{i3}^{(n)}\bar{u}_i^{(n)^*})\mathrm{d}s,\quad n=1,2,3, \tag{5}$$

where ω is the circular frequency, W is the aperture, s_n is the cutoff slowness of the nth bulk wave, and B_n, $D_3^{(n)}$, $\varphi^{(n)}$, $T_{i3}^{(n)}$ and $\bar{u}_i^{(n)}$ are the coefficients in the linear combination of partial waves, electric displacement, potential, stress, and mechanical displacement associated with the nth bulk waves in s domain, respectively. We have calculated the distributions of stress and free charge in space using FEM/BEM, their counterparts in s domain can be given by performing a Fourier transform,

$$\begin{bmatrix}\bar{t}_s(s)\\ \bar{\sigma}(s)\end{bmatrix}=\pi\sum_{j=1}^{N}a_j\mathrm{e}^{\mathrm{j}\omega s c_j}\sum_{n=1}^{N_{ch}}\begin{bmatrix}\boldsymbol{b}_{t_s}\\ b_\sigma\end{bmatrix}_n j^nJ_n(\omega s a_j), \tag{6}$$

where $J_n(\cdot)$ represents Bessel function of the first kind. Utilizing the theory described in Ref.[8], B_n can be calculated from the distributions of stress and free charge in s domain. Once the radiation power of each bulk wave is obtained, it is easy to extract their contributions to overall input conductance, respectively. This may give an important insight into SAW devices.

The computation of the bulk wave power can be simplified by introducing a concept of generalized resistance densities. On the surface of substrate, let $x_3=0$, the displacements and potential can be written in a matrix form[8].

$$\begin{bmatrix}\bar{u}_1\\ \bar{u}_2\\ \bar{u}_3\\ \varphi\end{bmatrix}=\begin{bmatrix}\bar{u}_1^{(1)} & \bar{u}_1^{(2)} & \bar{u}_1^{(3)} & \bar{u}_1^{(4)}\\ \bar{u}_2^{(1)} & \bar{u}_2^{(2)} & \bar{u}_2^{(3)} & \bar{u}_2^{(4)}\\ \bar{u}_3^{(1)} & \bar{u}_3^{(2)} & \bar{u}_3^{(3)} & \bar{u}_3^{(4)}\\ 1 & 1 & 1 & 1\end{bmatrix}\begin{bmatrix}B_1\\ B_2\\ B_3\\ B_4\end{bmatrix}. \tag{7}$$

From the motion equations and piezoelectric constitutive equations[8], we can obtain

$$\begin{bmatrix}T_{13}\\ T_{23}\\ T_{33}\\ D_3\end{bmatrix}=\begin{bmatrix}T_{13}^{(1)} & T_{13}^{(2)} & T_{13}^{(3)} & T_{13}^{(4)}\\ T_{23}^{(1)} & T_{23}^{(2)} & T_{23}^{(3)} & T_{23}^{(4)}\\ T_{33}^{(1)} & T_{33}^{(2)} & T_{33}^{(3)} & T_{33}^{(4)}\\ D_3^{(1)} & D_3^{(2)} & D_3^{(3)} & D_3^{(4)}\end{bmatrix}\begin{bmatrix}B_1\\ B_2\\ B_3\\ B_4\end{bmatrix}. \tag{8}$$

The left hand side of Eq.(8) can be obtained from Eq.(6) and electrical boundary conditions, details of calculating the matrix on the right hand side of Eq.(8) have been given in Ref.[8]. Define a frequency-independent matrix as

$$\boldsymbol{T}=-\mathrm{j}k\begin{bmatrix}T_{13}^{(1)} & T_{13}^{(2)} & T_{13}^{(3)} & T_{13}^{(4)}\\ T_{23}^{(1)} & T_{23}^{(2)} & T_{23}^{(3)} & T_{23}^{(4)}\\ T_{33}^{(1)} & T_{33}^{(2)} & T_{33}^{(3)} & T_{33}^{(4)}\\ D_3^{(1)} & D_3^{(2)} & D_3^{(3)} & D_3^{(4)}\end{bmatrix}^{-1}. \tag{9}$$

In the following derivation, D_3 will be written as T_{43} for convenience. From Eqs.(8) and (9), we have

$$B_n=-\frac{1}{\mathrm{j}k}\sum_{i=1}^{4}T_{ni}T_{i3}. \tag{10}$$

Substituting Eq.(10) into Eq.(5), we obtain

$$p_n=W\omega\sum_{k=1}^{4}\sum_{l=1}^{4}\frac{1}{4\pi}\mathrm{Re}\int_{-s_n}^{s_n}-\frac{1}{s}T_{nk}T_{nl}T_{k3}T_{l3}^{*}Q^n\mathrm{d}s, \tag{11}$$

where $Q^n=\frac{\mathrm{j}}{k}\left(D_3^{(n)}\varphi^{(n)^*}+\sum_{i=1}^{3}T_{i3}^{(n)}\bar{u}_i^{(n)^*}\right)$, Q^n is also frequency-independent.

Define

$$R_n^{kl}=-\frac{1}{4\pi s}T_{nk}T_{nl}Q^n,\quad n=1,2,3 \tag{12}$$

as generalized resistance densities, so that the power radiated into substrate for the nth bulk wave can be rewritten as:

$$p_n=W\omega\mathrm{Re}\left(\sum_{k=1}^{4}\sum_{l=1}^{4}\int_{-s_n}^{s_n}R_n^{kl}T_{k3}T_{l3}^{*}\mathrm{d}s\right). \tag{13}$$

Compared with the resistance density defined as a scalar in Ref.[5], the merit of generalized resistance densities R_n^{kl} defined in this paper is that the effect of mass loading is included. In general, they can be written as three 4×4 tensors, each of which represents a bulk wave. As the dyadic Green's function, R_n^{kl} only depend on the substrate orientation and therefore need to be evaluated only once for a given cut. They relate the power of radiated bulk wave with the distributions of stresses and free charge directly. Once the distributions of stress and charge are calculated, the powers of bulk waves can be obtained by Eq.(13), much faster than by Eq.(5).

From Eq.(13) the angular distribution of bulk wave can be derived using the method similar to the one described in Ref.[5],

$$\frac{\mathrm{d}p_n}{\mathrm{d}\theta_n} = W\omega \mathrm{Re}\left(\sum_{k=1}^{4}\sum_{l=1}^{4} R_n^{kl} T_{k3} T_{l3}^{*}\right) s_b^{(n)} \cos\theta_n, \tag{14}$$

where θ_n is the angle at which the wave vector is to the $-x_3$ axis, and $s_b^{(n)}$ is the actual bulk wave slowness parallel to the wave vector. The direction of the wave vector given in Eq. (14) is not appropriate to display the angular distribution of power. The power flow angle should be used. It is not difficult to calculate the relation between θ_n and energy flow angle φ_n by utilizing the slowness surface of bulk wave, so we can obtain the power distribution with energy flow angle $\mathrm{d}\theta_n/\mathrm{d}\varphi_n$ for the nth bulk wave.

3 Bulk wave radiations in a one-port resonator on 42° *Y*-rotated $LiTaO_3$

Figure 1 shows the simulated and experimentally measured conductances and susceptances of a 450 MHz synchronous one-port resonator. The device is fabricated on 42° *Y*-rotated $LiTaO_3$ with 119 Al-electrodes with height $h=6800$ Å, pitch $p=4.375$ μm, metallization ratio $\eta=0.6$, and aperture $W=119$ μm. Ohmic losses in electrodes and material losses are introduced in the simulation. Also, a small pad-to-pad capacitance is included to compensate for the anti-resonant frequency deviation[7]. The material parameters used in this paper are from Ref. [9]. Good agreement is obtained, although some differences exist in some frequency ranges, such as close to minimums of the input conductance below resonance, and from 450 MHz to 460 MHz between resonance and anti-resonance. The explanation of these discrepancies will be given in the next section.

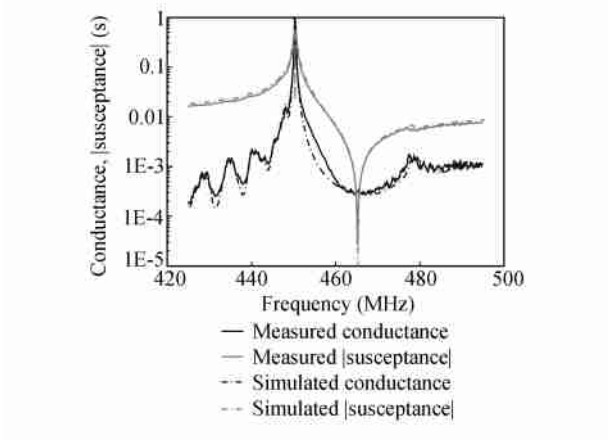

Fig. 1. Simulated and measured admittance of a 450 MHz synchronous one-port resonator.

Figure 2 shows the input conductance and the contributions of SSBAW, FSBAW and LBAW to input conductance for the same device. The relative contributions of three bulk waves to the input conductance are shown in Fig. 3. In this calculation no ohmic loss and material loss are included. In Fig. 2, the sum of contributions of SSBAW, FSBAW and LBAW is almost equal to the overall input conductance.

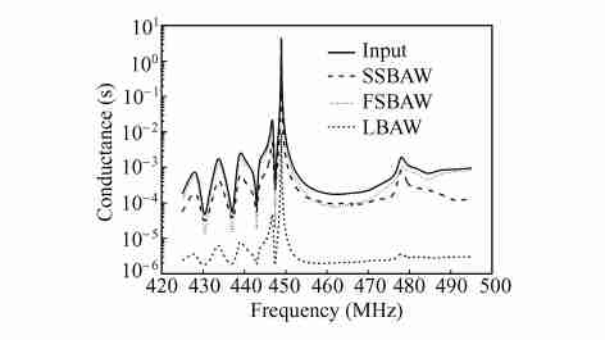

Fig. 2. Input conductance and the contributions of SSBAW, FSBAW and LBAW to input conductance for a synchronous one-port resonator.

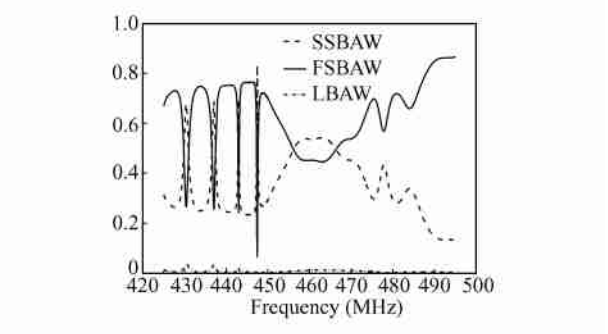

Fig. 3. The relative contributions of SSBAW, FSBAW and LBAW to input conductance for a synchronous one-port resonator.

Figure 4 shows the calculated angular distributions of the normalized powers of SSBAW, FSBAW and LW at 447 MHz slightly below resonance. The bulk waves radiate symmetrically into substrate in the foreward and backward directions. SSBAW radiates into substrate at an angle of about 40.3° with the suface and features a very concentrated directivity, which can be verified by the experimental results in Ref. [10]. The FSBAW propagates at an angle of about 1.3° with the surface. The maximum lobe of LW is at an angle of about 8.5° with the surface.

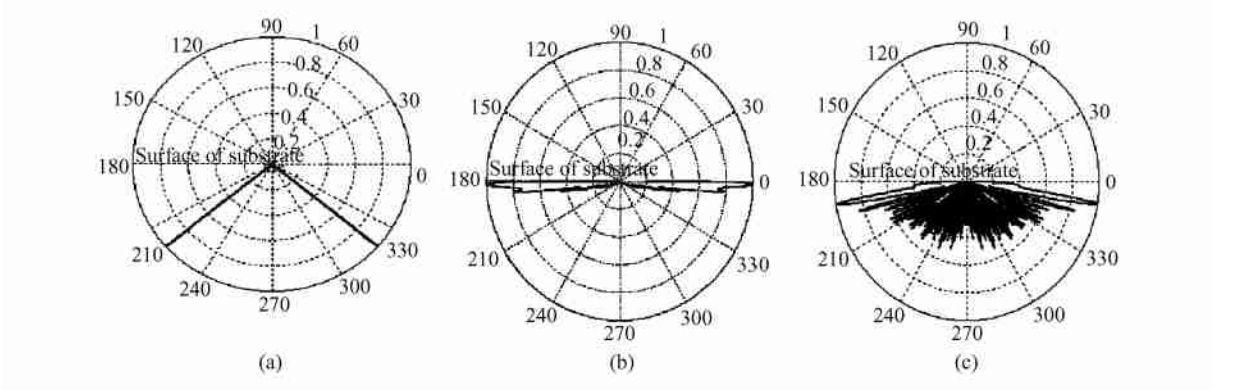

Fig. 4. The angular distributions of the normalized powers of (a) SSBAW, (b) FSBAW and (c) LBAW for a synchronous one-port resonator on 42° *Y*-rotated $LiTaO_3$ at 447 MHz.

4 Discussion

The simulation is deviated from measurement mainly in two regions:

(i) Close to minimums of the input conductance below resonance and at anti-resonant frequency as shown in Fig. 1. As we can see from Figs. 2 and 3, these frequency regions are just the same region where SSW occupies a large portion. From Fig. 4 we know that SSBAW radiates into substrate under a large angle. Therefore, we can infer that even though the bottom is treated to avoid bulk wave reflection, it is difficult to avoid bulk wave reflection completely. As a result of reflection of SSBAW, the measured conductance would be larger.

(ii) From 450 MHz to 460 MHz between resonance and anti-resonance as shown in Fig. 1. Reference [11] indicated a 3D effect, LSAW will leak into busbar in this frequency region. The simulation in this paper does include 3D effect.

With the method described in this paper, one can reveal more details about the loss of the devices, the distributions of the loss among three bulk wave modes and the angle distributions of bulk waves radiated into the substrate. It provides a powerful tool for the analysis of SAW devices.

Acknowledgment The authors would like to thank the GVR Trade SA Company (in Switzerland) for providing the experimental data used in this paper.

References

1 Koskela J. and Plessky V. P. Suppression of the Leaky SAW attenuation with heavy mechanical loading. IEEE transactions on Ultrasonics, Ferroelectrics, and Frequency Control, 1998, 45(2): 439—449.

2 Hashimoto K. Y., Yamaguchi M., Mineyoshi S. et al. Optimum leaky-SAW cut of $LiTaO_3$ for minimised insertion loss devices. In: Proceedings of the IEEE Ultrasonics Symposium, 1997, 245—254.

3 Takamine Y. C. U. S. patent, 6 621 380 B2, 2003-9-16.

4 Thomas B., Gunter K., Ulrike R. et al. U.S. patent, 6 420 946 B1, 2002-07-16.

5 Milsom R. F., Reilly N. H. C. and Redwood M. Analysis of generation and detection of surface and bulk acoustic waves by interdigital transducers. IEEE Transactions on Sonics and Ultrasonics, 1977, 24(3): 147—166.

6 Ventura P., Hode J. H. and Lopes B. Rigorous analysis of finite SAW devices with arbitrary electrode geometries. In: Proceedings of the IEEE Ultrasonics Symposium, 1995, 257—262.

7 Gamble K. J. and Malocha D. C. Simulation of short LSAW transducers including electrode mass loading and finite finger resistance. IEEE Transactions on Ultrasonics, Ferroelectrics, and Frequency Control, 2002, 49(1): 47—56.

8 Qiao D. H., Liu W. and Smith P. M. General Green's functions for SAW device analysis. IEEE transactions on Ultrasonics, Ferroelectrics, and Frequency Control, 1999, 46(5): 1242—1253.

9 Kovacs G., Anhorn M., Engan H. E. et al. Improved material constants for $LiNbO_3$ and $LiTaO_3$. In: Proceedings of the IEEE Ultrasonics Symposium, 1990, 435—438.

10 Knuuttila J. V., Koskela J., Vartiainen J. et al. BAW radiation from LSAW resonators on lithium tantalate. In: Proceedings of the IEEE Ultrasonics Symposium, 2001, 193—196.

11 Koskela J., Knuuttila J. V., Makkonen T. et al. Acoustic loss mechanisms in leaky SAW resonators on lithium tantalate. IEEE Transactions on Ultrasonics, Ferroelectrics, and Frequency Control, 2001, 48(6): 1517—1526.